SCANNING VOL. 9999, 1–7 (2016)

Cyclic Fatigue Resistance, Torsional Resistance, and Metallurgical Characteristics of DCTaper 2 and DCTaper 2H Rotary NiTi Files

S. W. Chang,[1] K. S. Shim,[1] Y. C. Kim,[2] K. K. Jee,[3] Q. Zhu,[4] H. Perinpanayagam,[5] and K. Y. Kum[6]

[1]Department of Conservative Dentistry, School of Dentistry, Kyung Hee University, Seoul, Korea
[2]Biomedical Research Institute, Korea Institute of Science and Technology, Seoul, Korea
[3]Future Convergence Research Division, Korea Institute of Science and Technology, Seoul, Korea
[4]Division of Endodontology, Department of Oral Health and Diagnostic Sciences, School of Dental Medicine, University of Connecticut Health Center, Farmington, Connecticut
[5]Schulich School of Medicine and Dentistry, University of Western Ontario, London, Canada
[6]Department of Conservative Dentistry, Dental Research Institute and BK21 Program, Seoul National University Dental Hospital, Seoul National, University School of Dentistry, Seoul, Korea

Summary: The aim of this study was to compare the cyclic fatigue resistance, torsional resistance, and metallurgical characteristics of conventional NiTi wire (DCTaper 2, DC2) and CM wire (DCTaper 2H, DC2H)-based files. Cyclic fatigue and torsional resistance of DC2 and DC2H were investigated by measuring the number of cycles to fracture, maximum torque at fracture, and maximum angle at fracture. The typical patterns of fatigue and torsional fractures were investigated using a scanning electron microscope (SEM). The metallurgical characteristics were investigated by differential scanning calorimetry (DSC) from −100 °C to 100 °C. The austenite finishing temperature (Af) of each instrument was also measured. The microstructures of the instruments were investigated by a transmission electron microscope (TEM) along with selected area diffraction pattern analysis. The results were statistically analyzed by Mann–Whitney U-test ($p = 0.05$). DC2H showed significantly higher cyclic fatigue resistance and torsional resistance than DC2. SEM images of the fractured surfaces showed typical patterns of fatigue and torsional fracture. The DSC analysis of DC2 showed one small peak in both the heating and cooling curves. The Af of DC2 was −0.32 °C. DC2H showed two remarkable peaks in the heating curve and one remarkable peak in the cooling curve. The Af of DC2H was 33.25 °C. The TEM analysis showed that both DC2 and DC2H are mainly composed of austenite. In conclusion, DC2H showed higher cyclic fatigue resis-tance and torsional resistance than DC2. The superior properties of DC2H could be attributed to the annealing effect and possibly the martensite phase. SCANNING 9999:1–7, 2016. © 2016 Wiley Periodicals, Inc.

Key words: cyclic fatigue resistance, thermal characteristics, torsional fracture resistance, DCTaper, DCTaper 2H

Introduction

In endodontic treatment, the complex root canal anatomy poses a challenge for root canal cleaning and shaping. In fact, most root canals have varying degrees of curvatures and anatomical danger zones which make root canal cleaning and shaping even more difficult. In these canals, the use of conventional stainless steel files is limited by their stiffness and they are less likely to maintain the original canal center and avoid transportation.

NiTi rotary files were introduced to the field of endodontics in the early 1990s (Walia et al., ’88). Since they possess superior flexibility and super-elasticity, NiTi files are more likely to maintain the original canal center than stainless steel hand files. However, NiTi rotary files still inadvertently transport canals, particularly when less flexible or aggressively cutting files are used. Furthermore, conventional NiTi files can be separated within root canals due to cyclic fatigue or

Contract grant sponsor: Ministry of Knowledge Economy (MKE, Korea).
Conflicts of interest: None.
Address for reprints: Kee-Yeon Kum, Department of Conservative Dentistry, Dental Research Institute, School of Dentistry, Seoul National University, Seoul 03080, Korea.
E-mail: kum6139@snu.ac.kr

Received 22 November 2015; revised 31 December 2015; Accepted with revision 7 January 2016

DOI: 10.1002/sca.21301
Published online XX Month Year in Wiley Online Library (wileyonlinelibrary.com).

torsional stress (Sattapan et al., 2000). The separated files that are lodged within infected canals can hinder root canal disinfection and thereby cause treatment failure (Spili et al., 2005).

Therefore, there have been multiple attempts to develop NiTi files that are less likely to transport and more resistant to fracture. Prior attempts have utilized electropolishing (Bui et al., 2008), ion implantation (dos Santos et al., 2012), surface coating, and heat treatment (Braga et al., 2014; Chang et al., 2013). Recent attempts have used thermal treatments (Shen et al., 2013) to modify the phase transition temperatures (Gutmann and Gao, 2012) and thereby enhance the mechanical properties of the files (Gutmann and Gao, 2012).

Recently, controlled memory (CM) wire-based NiTi rotary files were developed and introduced to the market. The manufacturers claim that the flexibility and resistance to fatigue/torsional stress of CM wire-based files are substantially enhanced. A previous study reported that CM wire-based instruments have superior cyclic fatigue resistance than conventional NiTi files (Shen et al., 2011a). However, the mechanism underlying their improved mechanical strength and flexibility are largely unknown. The aim of this study was to compare the cyclic fatigue and torsional resistance of CM wire-based NiTi rotary files (DCTaper 2H, DC2H) and conventional NiTi wire-based files (DCTaper 2, DC2), and to examine their thermomechanical and metallurgical properties.

Materials and Methods

Cyclic Fatigue Testing

The resistance to cyclic fatigue was measured in conventional NiTi wire-based DCTaper 2 (n = 12) (DC2; #25, SS White, Lakewood, CA) and CM wire-based DCTaper 2H (n = 12) (DC2H; #25, SS White) rotary instruments by using a cyclic fatigue tester (Denbotix, Bucheon, Korea). Each instrument was mounted on an electric torque-controlled motor (Aseptico, Woodin-ville, WA) which had a reduction (20:1) handpiece and was rotated at the manufacturer's recommended speed (300 rpm) inside an artificial canal (Fig. 1(A)), 1.5 mm diameter, 60° curvature, 5 mm radius) with a pecking movement (6 mm at 0.5 cycles per second). The artificial canals were filled with RC-prep (Premier Dental Products, Norristown, PA) to reduce friction and to dissipate generated heat. When the instrument was fractured within the canal, there was a change in torque detected by an internal sensor that immediately stopped the motor and recorded the time elapsed. The occurrence of a fracture was verified by visual examination. The number of cycles to failure (NCF) was calculated as a product of the time elapsed and the rotation rate (rpm). Using the SPSS statistics 23 (SPSS, Chicago, IL), the NCF of the two groups were analyzed by Mann–Whitney U-test applying a signifi-cance level of 0.05.

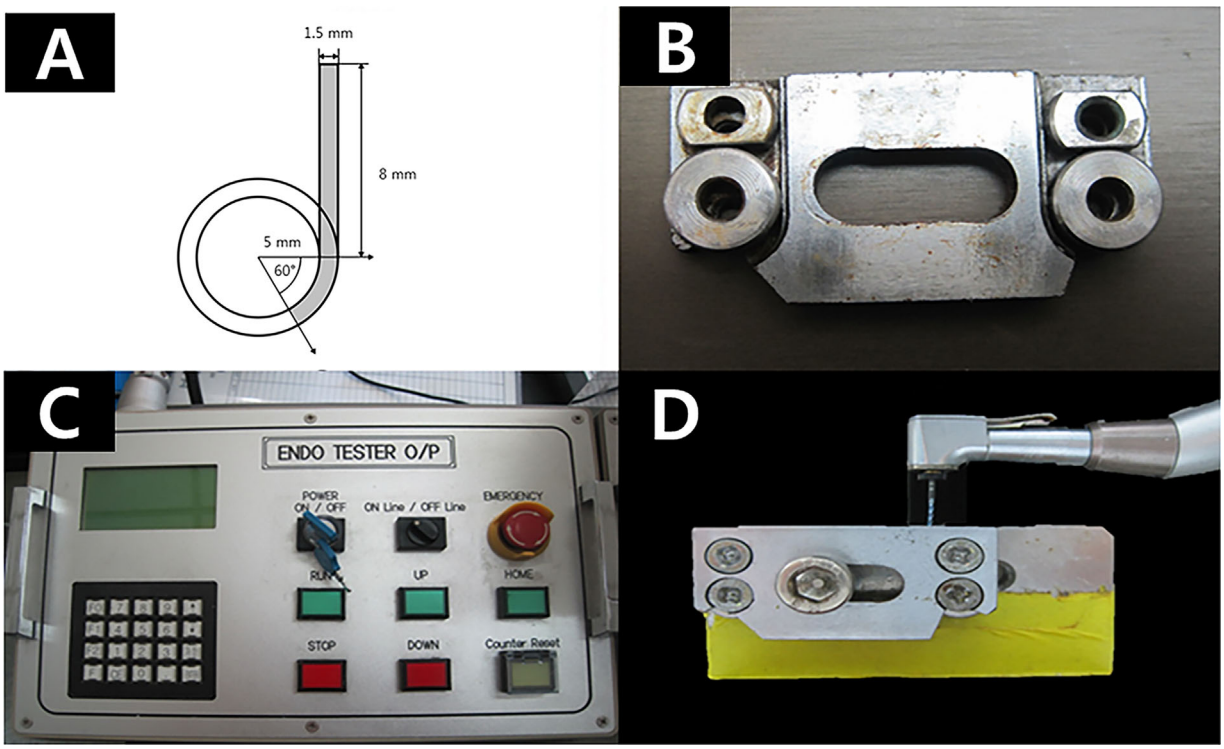

Fig 1. (A) A schematic diagram of the canal system. (B) Photograph of an artificial canal. (C) Photograph of the Endo Tester (D). A NiTi rotary file is rotated in a simulated canal with pecking motion.

Torsional Resistance Test

The tip of each file (n = 12) was fixed to a jig in a torque tester (Vortex-i, Mecmesin Co., Slinfold, U.K.). The files were subjected to clockwise rotation at 2 rpm. The torque and angular distortion were recorded until fracture occurred. The results were then statistically analyzed by Mann–Whitney U-test applying a significance level of 0.05.

Scanning Electron Microscopy (SEM) Analysis

The overall design of untreated DC2 and DC2H instruments were evaluated by SEM. In addition, the fractured surfaces were examined to investigate the characteristic features related to cyclic fatigue fracture and torsional fracture.

Differential Scanning Calorimetry (DSC)

The thermal behaviors of the DC2 and DC2H instruments were measured by DSC (TA Instruments, New Castle, DE). Small segments of the files were placed in an aluminum pan on a platinum holder inside the DSC measuring chamber. An empty pan was also evaluated as a reference. The chamber was filled with high purity argon gas to minimize oxidation. The exothermic or endothermic energy flow was recorded by raising the temperature to 100 °C followed by subsequent cooling to −100 °C and re-heating to 100 °C. The coolant used in this experiment was liquid nitrogen. The heating and cooling rate was 0.17 °C/s. The austenite transformation finishing points (Af) were determined.

Transmission Electron Microscopy (TEM) With Selected Area Diffraction Analysis (SADA)

For TEM analysis, samples were prepared by a dual beam focused ion beam (DB-FIB) (Helios Nanolab 600, FEI, Hillsboro, OR). The DB-FIB system contains an ion column with a liquid ion source of gallium (Ga+) for sectioning and a Schottky field emission electron column for imaging. Uniform and damage-free TEM samples were obtained with a thickness of less than 100 nm using variable accelerating voltages between 1 and 30 kV. SADA was also performed. The microstructural analysis was carried out by using a 200 kV TECNAI F20 G2 SuperTwin TEM (FEI, Hillsboro, OR) with the sample mounted in a double-tilt holder (Gatan Inc., Pleasanton, CA). TEM images were obtained by an UltraScan 1000 (2k × 2k) CCD camera (Gatan Inc.) and a Fischhione Model 3000 ADF detector. Qualitative and quantitative compositional analyses were performed using energy dispersive spectroscopy (EDX PV9761, AMETEK, Inc., Berwyn, PA).

Results

Resistance to Torsional Fracture and Cyclic Fatigue

DC2H had a significantly higher cyclic fatigue resistance (6,392.80 ± 2,100.00) than DC2 (984.50 ± 135.64) ($p < 0.05$) (Table I). DC2H also had a significantly higher distortion angle (946.37°) at break than DC2 (581.58°) ($p < 0.05$) but the maximum torque values were not significantly different (Table I).

SEM Analysis

Overall, the SEM images of both untreated instruments revealed non-cutting tips (Fig. 2(A): DC2 and (B): DC2H). No unwinding or distortion of the files resulted from the cyclic fatigue fractures (Fig. 2(C): DC2 and (D): DC2H). However, torsional fracture resulted in distortion and unwinding of the files (Fig. 2(E): DC2 and (F): DC2H). The fatigue-fractured surfaces revealed characteristic patterns of fatigue fractures (Fig. 2(G): DC2 and (H): DC2H) including multiple striations (Fig. 2(I and J)(magnification of white box in Fig. 2(I))), multiple dimples (Fig. 2(K)), and microcracks (black arrow in Fig. 2(L)) initiated from the lateral surfaces of the instruments. Torsional-fractured surfaces showed typi-cal patterns of torsional fractures such as circular abrasion marks as well as deformation and distortion around the fractured surfaces (Fig. 2(M and N)).

Differential Scanning Calorimeter Analysis

The differential scanning calorimeter (DSC) pattern of DC2 showed a small endothermic peak

TABLE I Cyclic fatigue and torsional resistance values of DC2 and DC2H (mean ± SD)

	NCF	Maximum torque	Angle at fracture
DCTaper	984.50 ± 135.64*	2.45 ± 0.71	581.58 ± 208.33*
DCTaper 2H	6,392.80 ± 2,100.00*	2.19 ± 0.33	946.37 ± 85.69*

NCF, number of cycles to fracture. Asterisk (*) means statistically significant difference within column.

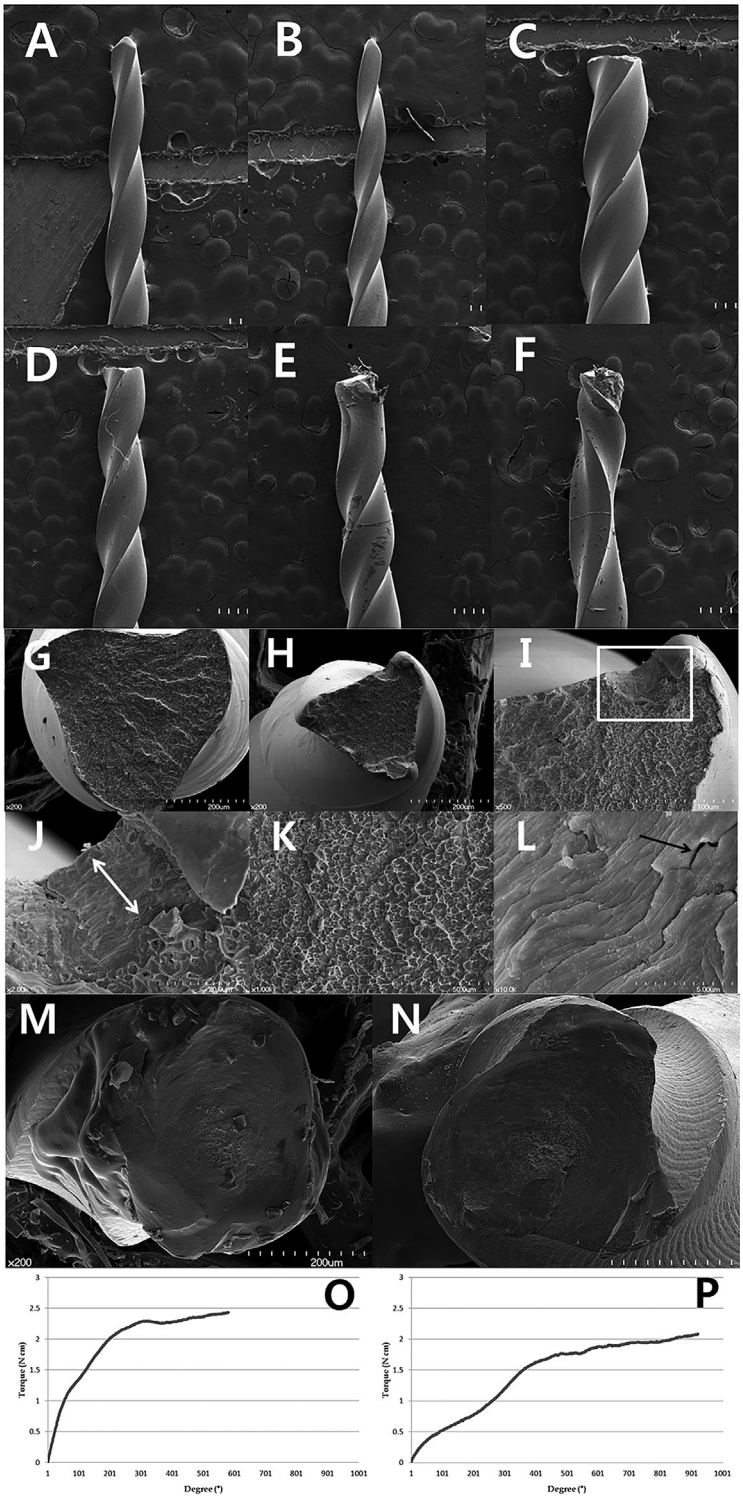

Fig 2. Overall view of the (A) DC2 and (B) DC2H NiTi rotary files which had non-cutting tips. The cyclic fatigue-fractured instrument (C: DC2, D: DC2H) revealed that the flutes were neither distorted nor unwinded. Torsion-induced fractures produced unwinding and distortions of the files (E: DC2, F: DC2H). Cyclic fatigue-fractured surfaces of DC2 (G) and DC2H (H–L). The fractured surfaces showed characteristic features of cyclic fatigue fractures including multiple striations (I). (J) is the magnification of white box in (I). White double-headed arrow in (J) shows multiple striations. (K) shows multiple dimples. (L) shows the microcracks (black arrow in (L)). Torsion-fractured surfaces of DC2 (M) and DC2H (N). Both images reveal a circular abrasion mark that represents typical patterns of torsional fractures. Strain–stress curves showing that DC2H (P) had a greater distortion angle at fracture than DC2 (O).

and a barely observable exothermic peak, which imply that DC2 did not receive thermal treatment (Fig. 3(A)). On the contrary, DC2H revealed significant endothermic and exothermic peaks (Fig. 3(B)), which imply that DC2H received thermal treatment. The DSC curve for DC2 exhibited a single and defined peak upon cooling and heating. This peak represents the martensitic and reverse transformation between austenite and martensite. The Af temperatures for DC2 were lower than room temperature (−0.32˚), which means that at room temperature, DC2 is almost completely an austenite phase. On the contrary, in the DSC curve of DC2H, double endothermic peaks in the heating (upper) curve represent the transformation from a martensite to an intermediate R-phase, followed by transformation from the intermediate R-phase to an austenite phase. The austenite-finish temperature was higher than room temperature (33.25 ˚C), which implies that at room temperature, DC2H is composed of a mixture of austenite and the intermediate R-phase.

Transmission Electron Microscopy Examination and Selected Area Diffraction Pattern Analysis

On the surface of the DC2 instrument, only an inner NiTi layer and TiO_2 layer were identified. The TiO_2 layer is 5–10 nm thick (Fig. 3(C), white arrow), continuous, and has a uniform thickness (Fig. 3(D and E), white arrows). The grain size is about 100 nm. The morphology of the NiTi grains is round or spindle-shaped (Fig. 3(F)). SADA of the internal microstructure of DC2 revealed that the internal structure of DC2 is almost completely composed of a NiTi BCC phase (austenite)(Fig. 3(G and H)).

On the surface of DC2H, three layers were identified. The outermost surface is a TiO_2 layer (Fig. 3(I), black arrow), the second layer is a Ni_3Ti layer (Fig. 3(I), white-closed arrow), and the innermost layer is a NiTi layer (Fig. 3(I), white-open arrow). These three layers were confirmed by EDS analysis (Fig. 3(J)). The size of the NiTi grains increased from the surface to the inside. The grain sizes were 100 nm at the surface (Fig. 3(K),

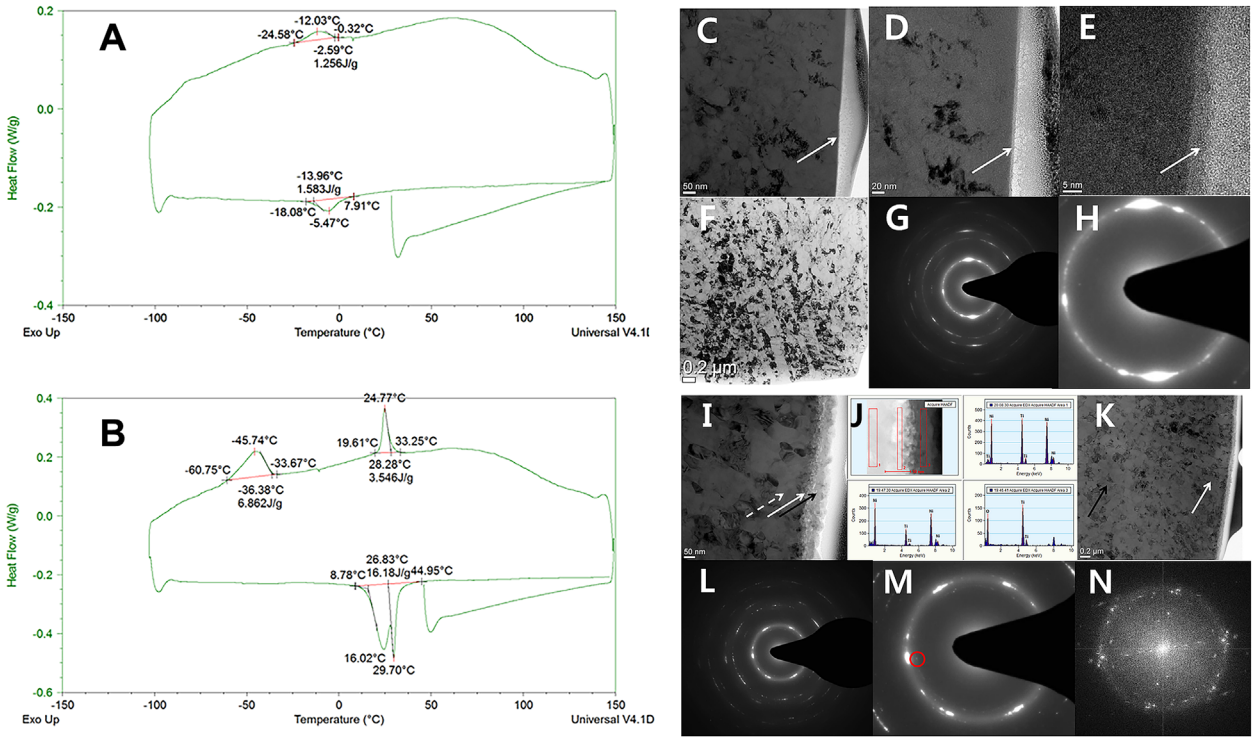

Fig 3. (A) DSC result of DC2 showed small endothermic and exothermic peaks. (B) However, DC2H showed remarkable endothermic and exothermic peaks. The surface of DC2 (white arrow in C–E) revealed a continuous TiO_2 outermost layer with a uniform thickness of 5–10 μm. (F) The internal structures of DC2 are composed almost entirely of a BCC (austenite) phase. The grain size of DC2 was about 100 nm. The DC2 NiTi grains were round or spindle-shaped (F). The SADA pattern (G and H) confirmed that the internal structures of DC2 are almost entirely composed of a NiTi BCC phase. The surface of (I) DC2H had three layers (TiO_2 (black arrow), Ni_3Ti (closed white arrow), and NiTi (open white arrow)). (J) The results of the EDS analysis confirmed the existence of these three layers. (K) The size of the NiTi grains increased from the surface (white arrow) to the inside (black arrow). (L) SADA of the internal microstructure of DC2H revealed that DC2H is mainly composed of a NiTi B2 phase (austenite). A small fraction of the B19 phase, which is postulated to be martensite, was also identified (red circle (M)). (N) Intensive examination of the Ni_3Ti layer revealed that this layer has a grain size of approximately 10 nm and is possibly composed of a B19 phase (martensite) or Ni_3Ti.

white arrow) and 200 nm in the inner area (Fig. 3(K), black arrow). SADA of the internal microstructure of DC2H revealed that the internal structure of DC2H is mainly composed of a NiTi B2 phase (austenite) (Fig. 3(L)). Other than the B2 phase, a small fraction of a B19 phase was also identified, which is postulated to be Ni_3Ti or martensite (red circle in Fig. 3(M)). Intensive examina-tion of the Ni_3Ti layer revealed that this layer has a grain size of approximately 10 nm and is possibly composed of a B19 phase (martensite) or Ni_3Ti (Fig. 3(N)).

Discussion

A couple of previous studies demonstrated that M wire-based NiTi rotary instruments have superior fatigue resistance compared to conventional NiTi wire-based instruments (Gao et al., 2012; Ye and Gao, 2012). Another study reported that a CM wire-based instrument (Hyflex) was more flexible and resistant to cyclic fatigue than conventional NiTi alloy or M wire-based instru-ments (Pongione et al., 2012). However, very few studies have examined the underlying mechanism for the superior mechanical characteristics of CM wire-based instruments (Shen et al., 2011b). The only study which has examined the thermomechanical behavior of CM wire-based instruments was conducted by Shen et al.(2011a). They reported that a CM wire-based instrument (Typoon) has an Af above room temperature, so that mixed phases of austenite and martensite are present at room temperature. This suggests a mechanism for the superior mechanical properties in CM wire-based instruments, but requires a detailed examination of their internal microstructure using TEM and SADA for confirmation.

Therefore, the present study used several metallurgical laboratory techniques including DSC, SEM, TEM, EDS, and SADA to perform an in-depth comparison of the mechanical properties and metallurgical characteristics of NiTi rotary instruments made from two types of NiTi wires. The instruments were DC2 rotary files that are based on traditional NiTi wire and a revised version, DC2H, manufactured from CM wire. This detailed examination of the DC2 and DC2H files by TEM and SADA is the first report for any CM wire-based instruments.

In this study, it was found that the DC2H files had a significantly higher NCF than DC2. This may be due to the properties of CM wire, which is reported to be more flexible than conventional NiTi wires (Plotino et al., 2014). Additionally, in torsional strength tests, DC2H had much higher distortion angles at its breaking point than the DC2 files (Fig. 2(O and P)), which may also be attributed to the CM wire. The subsequent SEM analysis of the fractured surfaces showed that they possessed typical characteristics of cyclic fatigue and torsional stress.

There were remarkable differences in the DSC results between the DC2 and DC2H instruments. Distinct endothermic and exothermic peaks were absent from the curves for DC2, which suggests that they had not been subjected to any thermal treatment. On the other hand, multiple peaks were observed in the DSC curve of DC2H, which suggests that they received thermal treatment. This thermal treatment of DC2H could have improved the cyclic fatigue and torsional resistance in two possible ways. First, the thermal treatment could anneal and reduce the residual internal stress produced in mechanical processes like milling. Annealing has been widely utilized to reduce residual stresses and improve the flexibility of metallic instruments (Chang et al., 2013). Secondly, as a result of thermal treatment, DC2H had an Af of 33.25 °C. These results imply that at room tempera-ture, an R-phase or martensite phase could be mixed with an austenite phase in DC2H. On the contrary, the DSC results of DC2 revealed an Af of −0.32 °C, which implies that DC2 is almost entirely composed of an austenite phase at room temperature. Considering that the martensite phase could endow flexibilities in NiTi rotary instruments (Pereira et al., 2012), the mixture of a martensite phase in DC2H could partly explain the increased cyclic fatigue resistance and torsional resistance.

The TEM analysis of DC2 and DC2H also revealed remarkable differences among the samples. DC2 had a surface TiO_2 layer and an inner NiTi layer. However, DC2H had an outermost TiO_2 layer, an intermediate Ni_3Ti layer, and an innermost NiTi layer. These differences could be attributed to the thermal treatment of DC2H. TiO_2 is a very effective and self-healing barrier against the release of Ni, which is known to be an allergen and carcinogen (Min et al., 2009). The TiO_2 layer may also protect the NiTi instrument from the corrosive actions of NaOCl (Cheung and Darvell, 2008). Ni_3Ti is an intermetallic phase which could be produced as a result of thermal treatment (Tomihisa et al., 2002). The Ni_3Ti layer had small grain sizes of approximately 10 nm. The SADA pattern analysis revealed that the internal structure of DC2 is mostly composed of a NiTi BCC phase (austenite) and the internal microstructure of DC2H is composed of a B2 phase (austenite) with a very small fraction of B19 (martensite). These results agree with the DSC analysis results.

Conclusion

Within the limitations of this study, DC2H showed significantly higher cyclic fatigue resistance and torsional resistance than DC2. These superior properties could be attributed to the annealing effect, internal stress relaxation effect, and possibly the martensite phase.

Acknowledgment

The authors thank Division of Biostatistics, Medical Science Research Center for their statistical consulting services. Yu-Chan Kim acknowledges the financial support of the Industrial Strategic Technology Development Program (10042703) funded by the Ministry of Knowledge Economy (MKE, Korea).

References

Braga LC, Faria Silva AC, Buono VT, de Azevedo Bahia MG. 2014. Impact of heat treatments on the fatigue resistance of different rotary nickel-titanium instruments. J Endod 40:1494–1497.

Bui TB, Mitchell JC, Baumgartner JC. 2008. Effect of electropolishing ProFile nickel-titanium rotary instruments on cyclic fatigue resistance, torsional resistance, and cutting efficiency. J Endod 34:190–193.

Chang SW, Kim YC, Chang H, et al. 2013. Effect of heat treatment on cyclic fatigue resistance, thermal behavior and microstructures of K3 NiTi rotary instruments. Acta Odontol Scand 71:1656–1662.

Cheung GS, Darvell BW. 2008. Low-cycle fatigue of rotary NiTi endodontic instruments in hypochlorite solution. Dent Mater 24:753–759.

dos Santos M, Gavini G, Siqueira EL, da Costa C. 2012. Effect of nitrogen ion implantation on the flexibility of rotary nickel-titanium instruments. J Endod 38:673–675.

Gao Y, Gutmann JL, Wilkinson K, Maxwell R, Ammon D. 2012. Evaluation of the impact of raw materials on the fatigue and mechanical properties of ProFile Vortex rotary instruments. J Endod 38:398–401.

Gutmann JL, Gao Y. 2012. Alteration in the inherent metallic and surface properties of nickel-titanium root canal instruments to enhance performance, durability and safety: a focused review. Int Endod J 45:113–128.

Min KS, Yang SH, Kim EC. 2009. The combined effect of mineral trioxide aggregate and enamel matrix derivative on odontoblastic differentiation in human dental pulp cells. J Endod 35:847–851.

Pereira ES, Peixoto IF, Viana AC, et al. 2012. Physical and mechanical properties of a thermomechanically treated NiTi wire used in the manufacture of rotary endodontic instruments. Int Endod J 45:469–474.

Plotino G, Testarelli L, Al-Sudani D, et al. 2014. Fatigue resistance of rotary instruments manufactured using different nickel-titanium alloys: a comparative study. Odontology 102:31–35.

Pongione G, Pompa G, Milana V, et al. 2012. Flexibility and resistance to cyclic fatigue of endodontic instruments made with different nickel-titanium alloys: a comparative test. Ann Stomatol (Roma) 3:119–122.

Sattapan B, Nervo GJ, Palamara JE, Messer HH. 2000. Defects in rotary nickel-titanium files after clinical use. J Endod 26:161–165.

Shen Y, Qian W, Abtin H, Gao Y, Haapasalo M. 2011a. Fatigue testing of controlled memory wire nickel-titanium rotary instruments. J Endod 37:997–1001.

Shen Y, Zhou HM, Zheng YF, et al. 2011b. Metallurgical characterization of controlled memory wire nickel-titanium rotary instruments. J Endod 37:1566–1571.

Shen Y, Zhou HM, Zheng YF, Peng B, Haapasalo M. 2013. Current challenges and concepts of the thermomechanical treatment of nickel-titanium instruments. J Endod 39:163–172.

Spili P, Parashos P, Messer HH. 2005. The impact of instrument fracture on outcome of endodontic treatment. J Endod 31:845–850.

Tomihisa K, Kaneno Y, Takasugi T. 2002. Phase relation and microstructure in Ni3Al-Ni3Ti-Ni3Nb pseudo-ternary alloy system. Intermetallics 10:247–254.

Walia HM, Brantley WA, Gerstein H. 1988. An initial investigation of the bending and torsional properties of Nitinol root canal files. J Endod 14:346–351.

Ye J, Gao Y. 2012. Metallurgical characterization of M-Wire nickel-titanium shape memory alloy used for endodontic rotary instruments during low-cycle fatigue. J Endod 38:105–107.